The High-Quality Precision Casting of Titanium Alloys

Ken-ichiro Suzuki

Author's Note: Unless otherwise indicated, compositions are given in weight percent.

A technique for the high-quality precision casting of titanium alloys has been developed that consists of the instantaneous dissociation of oxide at the metal-mold interface, followed by the rapid absorption and diffusion of the dissociated oxygen into the subsurface of the cast parts during solidification and cooling. In centrifugal casting trials using less molten alloy than required to completely fill the mold, the results suggest that the melt flowing in the mold cavities maintains contact with the vertical inside walls and directionally solidifies from the far end of the cavity to the gate, corresponding to the gradient in the centrifugal force on the horizontal plane. This force enhances the removal of defects, such as entrapped gas bubbles and solidification shrinkage. The results have enabled the development of a two-dimensional model to simulate melt flow during centrifugal casting.

INTRODUCTION

Titanium-alloy precision-cast parts are produced by vacuum-arc melting and centrifugal casting in a lost-wax mold made from materials that will not react with the molten titanium alloy. A shortcoming of parts cast in this manner is the lower fatigue strength as compared to machined and welded parts. A reason for this reduced performance is the presence of an oxygen-enriched hardened layer at the surface of the casting and porosity. The cast parts also have a nonuniform grain size.[1–3] To minimize the surface-hardened layer (SHL) and achieve the required mechanical properties in a Ti-6Al-4V casting, it is necessary to employ a combination of melting, molding, and heat-treating practices.[4–9]

ISSUES IN OXIDATION

Oxide Effects on Hardness

During the manufacture of a mold, a slurry solution, consisting of an oxide powder and binder, is coated several times on a wax model. Ultimately, it becomes a face coat of the precision-casting mold after dewaxing and high-temperature sintering. In order to evaluate the face-coating material (without the influence of the binder), the oxides SiO_2, Al_2O_3, ZrO_2, CaO, and Y_2O_3 (purity > 99.8) were plasma-sprayed up to thicknesses of 100 μm (±10) on a round-shaped cavity (40 mm$^{\phi}$ on top of a mullite block[5,6]). Next, 80 g of Ti-6Al-4V (6.3 Al, 4.1 V, and 0.19 O) was arc-melted in a copper crucible under high-purity argon and was poured into the cavity. Following solidification, microVickers hardness in the SHL was measured at 50 μm intervals on the vertical cross section of the ingot. The ingot temperature was measured at 0.4 mm from the bottom surface of the ingot using a Mo-Re thermocouple (0.2 mm$^{\phi}$). The temperature stayed between the liquidus and solidus temperatures for 1.2 seconds (±0.3) and decreased by 30 K/s (±5) at 1,223 K.

The characteristics of the plasma-sprayed oxide are classified into three groups.[6] In SiO_2, gaseous defects and marked α case were apparent in the SHL. Both the maximum hardness (H_V^{MAX}), 840, and the hardness in the bulk cast part (H_V^{INT}), 720, were substantially higher than the 340 hardness of the original alloy. In Al_2O_3, CaO, and ZrO_2, the H_V^{MAX} was 500–600, with α cases in the SHL. In Y_2O_3, the H_V^{MAX} was 380, and the thickness of the SHL (T_{SHL}) was 0.2 mm (the least among the oxides), with no noticeable change in the microstructure.

The hardness profiles in the SHL[6] are shown in Figure 1; similar oxygen profile trends are indicated. The oxygen-enrichment thickness was in good accordance with the T_{SHL} determined by the hardness profiles; however, the thicknesses of the metallic elements with oxides was limited to one-third of T_{SHL}. It was noted that Y_2O_3 is superior to the other oxides in the indices of H_V^{MAX}, H_V^{INT}, and T_{SHL}.[6]

Reactions taking place during casting are given by

$$MO_x(s) = M + (x/2)O_2(g)$$
$$MO_x(s) = \underline{M} + x\,\underline{O}$$
$$K_{MO} = a_M a_O$$

where $\underline{M}$ and $\underline{O}$ is M and O dissolved in molten Ti-6Al-4V, respectively.

The high-temperature stability of oxides can be estimated from the standard free-energy change;[10] however, stability against the molten alloy must be examined by taking the activities of $\underline{M}$ and $\underline{O}$ into account (i.e., the lower the activities, the further the given oxide dissociates). The free-energy change for the solution of M into molten titanium, $\Delta G^0{}_M{}^s$, was estimated by using the activity coefficients of $\underline{M}$ at the infinite dilution.[4] The free-energy change for the solution of $O_2(g)$ into the molten titanium alloy, $\Delta G^0{}_O{}^s$, is estimated by applying $p_O{}^2$ isotherms in the Ti-O system[11,12]

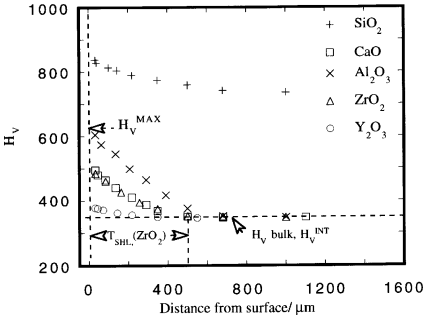

Figure 1. Hardness profiles in the SHL in the plasma-sprayed oxide layer.

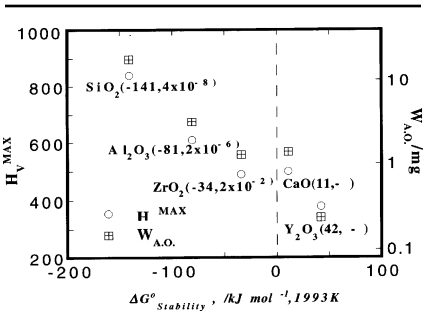

Figure 2. The relationship of H_V^{MAX}, $W_{A.O.}$, and $\Delta G^o{}_{Stability}$.

and by assuming the ideal behavior of the molten titanium alloy; $\Delta G^0_O{}^s$ was in good accordance with an extrapolated value of $\Delta G^0_O{}^s$ for Ti(s).[13]

$$(1/2)O_2(g) = \underline{O}$$

$$\Delta G^0_O{}^s = -RT\ \ln K_O = -354\ \text{KJ/mol}\ (1{,}993\ \text{K})$$

Thus, the standard free-energy change for the dissociation reaction can be calculated at 1,993 K by adding ΔG^0 for the formation of oxide,[11] $\Delta G^0_M{}^s$, and $\Delta G^0_O{}^s$, as shown by $\Delta G^0_{Stability}$ in Figure 2. The solubility product (Ca, O) for CaO was estimated as 6.3×10^{-2} at p_{Ar} of 5.1×10^4 Pa by referring to the solubility product 0.024 in Ti-6Al (l) under p_{Ar} of 2.1×10^4 Pa.[14] Because of the instability of CaO(s) under vacuum, CaO(s) may not be suitable for molds in the production of titanium-alloy cast parts with the higher quality specified by vacuum casting. The solubility product of Y_2O_3,[15] estimated in this study at 0.011, is comparable to 0.021 derived by Hoch et al.,[15] and 50 ZrO_2[2] to the 85 given by Saha et al.[16]

The effects of the stucco, filler, and binders contained in the slurry were evaluated by examining the alloy cast into a mold (20 mm$^\phi$, 40 mm^H) prepared after the ordinary slurry process. As expected, Y_2O_3 was superior to ZrO_2 as a filler or a stucco, and it was also noted that binders such as SiO_2 (14.1 wt.%) or TiO_2 (6.7 wt.%) in the face-coat layer increased H_V^{MAX}, H_V^{INT}, and T_{SHL}.[6] The allowable limits of impurities in a slurry consisting of Y_2O_3 filler and stucco were estimated by assuming the condition of $\Delta G^0_{Stability} > 0$. The contents of oxide impurities in the slurry should be held to levels lower than the following activity limits: 4×10^{-8} for SiO_2, 3×10^{-6} for TiO_2, and 2×10^{-6} for Al_2O_3.

In relation to the intense SHL in the cast parts poured into the SiO_2 layer, the partial pressure of SiO(g) evolved from SiO_2 was estimated at p_{O_2} of 10^{-16} Pa at 1,993 K and was compared with Al_2O(g) from Al_2O_3:

$$p_{SiO} = 18.0\ \text{Pa with the maximum of } 36{,}000\ \text{Pa at } p_{O_2} \text{ of } 10^{-9.4}\ \text{Pa}$$

$$p_{Al_2O} = 0.51\ \text{Pa with the maximum of } 1{,}040\ \text{Pa at } p_{O_2} = 10^{-14.0}\ \text{Pa}$$

During casting, p_{O_2} at the SiO_2 layer and Ti-6Al-4V interface may rapidly decrease to a level of $10^{-9.4}$ Pa, at which p_{SiO} attains the maximum. Accordingly, much of the SiO(g) evolved at the interface may yield gaseous defects at the surface and enrichment of the oxygen and silicon, even in the bulk of a cast part.[6] Meanwhile, gaseous defects may not be found in the case of Al_2O_3 because of the lower p_{Al_2O} and p_{O_2}.

The Thermochemical Stability of Oxides

Oxygen absorption and hardening at the surface of titanium-alloy cast parts may correlate to many factors, including

- A reaction between the molding material and the molten titanium alloy to evolve oxygen
- The absorption of oxygen into the alloy
- The diffusion of oxygen through the surface of the cast parts
- The partition of oxygen during solidification
- The solution hardening by the metallic element dissolved from the oxide

The effect of the last two factors has been experimentally confirmed to be negligibly small.[7,15]

A relation between H_V and the oxygen content in the alloy was determined for specimens with various oxygen contents based on the cooling rate[8] being kept at the same level as the titanium alloy in the mullite block.

Table I. An Estimation of Oxide Amounts Reacted with Ti-6Al-4V and of Oxygen Diffused into a Metal Layer

Oxide	H_V^{MAX}	T_{SHL} (mm)	Amount of Dissociated Oxide			Amount of Diffused Oxygen ($D_O t_{SHL}$ (cm^2) $\times 10^4$)
			$W_{oxygen}{}^+$	$W_{oxide}{}^+$	$T_{oxide}{}^{++}$	
SiO_2*	840	0.75	19	35	160	—
Al_2O_3	610	0.53	3.3	7.0	18	4.0
CaO	500	0.41	2.0	6.8	21	4.1
ZrO_2	490	0.40	1.8	6.4	11	4.4
Y_2O_3	380	0.33	0.36	1.7	3.8	4.0
Z-Z-Z†	560	0.57	2.1	8.1	14	5.0
Y-Z-Z†	510	0.40	1.0	4.2	8.6	3.6
Y-Z-Y†	420	0.35	0.53	2.5	5.4	2.9
Y-SiO_2-Y†	560	0.53	2.1	9.0	22	6.4
Y-TiO_2-Y†	450	0.46	0.83	3.8	8.4	6.1

\+ mg
++ μm
* Estimated by assuming an increase in HV is caused by oxygen dissociated from SiO_2 that is absorbed not only by the surface-hardened layer but also by the bulk of a cast.
† Set of filler, binder, and stucco in the order Y: Y_2O_3, Z: ZrO_2.

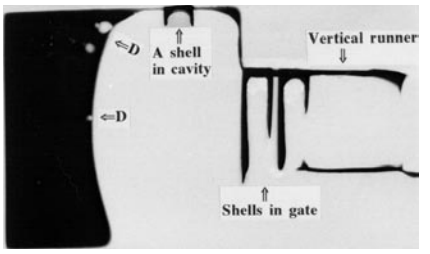

20 mm

Figure 3. A cross-sectional shape of a solidified shell in the flow pass of melt (200 rpm, 20% of melt) using x-ray radiography.

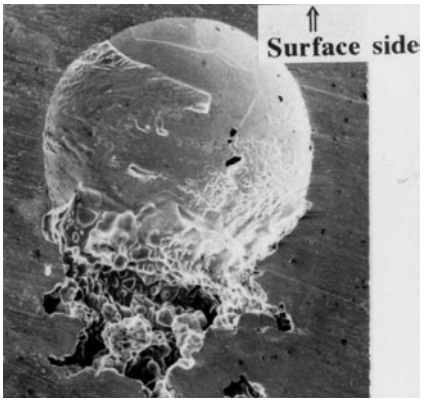

1 mm

Figure 4. A typical example of complicated defects with a smooth inside surface on the upper side and irregularity on the lower side of a cast part (100 rpm, 30% of melt).

Table II. The Effect of 20 G Centrifugal Force on Casting Defects Evaluated at the Dead End of the Cavity

Casting Mode	Centrifugal Casting	Static Casting
Minimum Thickness (t)	27 μm	190 μm
Diameter of Gaseous Defect (dB)	24 μm	90 μm
Critical Value of gL(-)	0.15	0.33 (assumed)
Diameter of Shrinkage Cavity	21 μm	32 μm (assumed)

$$[\text{wt.\% O}] = 9.6 \times 10^{-3} H_V - 3.10 \pm 0.10$$
$$(H_V: 343–600)$$

An integration of oxygen contents in the SHL estimated by use of the equation and measured hardness profiles yields the weight of the oxygen absorbed in the SHL. The weight and thickness of the oxide layer dissociated during casting can be estimated (Table I) by assuming no loss of oxygen and complete dissociation of the oxide at the interface. The thickness of oxides bringing about the SHL in cast parts, T_{oxide}, is less than 22 μm, except in SiO_2 (160 μm). The weight of oxygen absorbed in the SHL, W_{oxygen}, closely relates to the stability of oxides (Figure 2). From a practical viewpoint, T_{SHL} and H_V^{MAX} can be markedly reduced when Y_2O_3 is used as a face-coat material instead of ZrO_2, due to the reduction in the oxygen evolution to about one-fifth of that for ZrO_2.

The Diffusion of Oxygen

By assuming the diffusion coefficient of oxygen, D_O, is independent of oxygen content, the concentration of oxygen in the SHL at location x and time t [C(x, t)] is given by

$$d \ln C(x,t)/dx^2 = -(4D_O t)^{-1}$$

In the equation, x = 0 at the surface of a cast part, and t = 0 when the titanium alloy (l) contacts with the oxide. By a regression analysis of ln C(x) estimated from the H_V versus x^2 profiles in the SHL, the values of $(D_O t)_{SHL}$ can be obtained (Table I). Since oxygen diffuses from the surface to the inside of a cast part, oxygen diffusion is controlled at the surface, where temperature and, hence, the diffusion coefficient are lowest in the diffusion layer. Consequently, the value of $(D_O t)$ could be estimated by combining the temperature dependence of D_O with the interface temperature during casting, which was approximated at about –30 K/s at 0.4 mm apart from the interface.

By applying the temperature dependence of D_O reported by Rosa,[20] $(D_o t)_\alpha$ in the α phase (1,278 K to room temperature) is estimated to be negligibly small—$1/10^5$ of that in the β phase (solidification to 1,278 K) $(D_o t)_\beta$. The value of $(D_o t)_\beta$ thus estimated, however, cannot explain the experimental results. Instead, the similar relation proposed by Wasilewski et al.[21] and confirmed through an analysis of the surface layer of Ti-6Al-4V oxidized for 3,600 seconds at 1,323 K in air, was applied.

Through the linear regression analysis of $(D_O t)_{SHL}$ and W_{oxygen}, the following relation is derived:

$$(D_O t)_{SHL} = 0.0065\ W_{oxygen} + 0.0084$$
$$(n = 10, \text{correlation factor} = 0.99)$$

From these facts, one may assume that a $(Dt)_\beta$ of $2.9 \times 10^{-9} m^2$ always exists as solid-state diffusion for all oxides, and the $(D_o t)_l$ for the molten titanium alloy before solidification may change, corresponding to the stability of oxides. When the D_O in the molten titanium alloy is assumed as $10^{-4} m^2/s$, the time for oxygen diffusion from the plasma-sprayed layers into the molten alloy at the interface can be estimated to be 0.5 seconds for Y_2O_3, 1.2 seconds for ZrO_2, and 12 seconds for SiO_2. These values suggest that oxygen dissociation and absorption by the molten alloy may take place instantaneously and cease during solidification in the cases of Y_2O_3 and ZrO_2 because solidification time is 1.2 seconds (±0.3). In the case of SiO_2, however, oxygen absorption from SiO(g), taking place just after pouring the melt, may yield a lower concentration gradient of oxygen and, hence, a higher value of $(D_O t)_{SHL}$ and an erroneously longer time for oxygen diffusion in the liquid titanium-alloy phase.

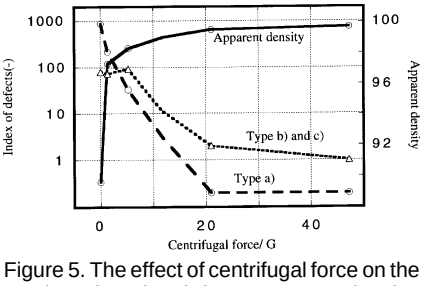

Figure 5. The effect of centrifugal force on the number of casting defects, apparent density, and tensile strength.

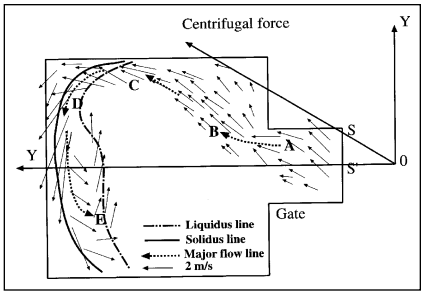

Figure 6. The flow pattern and progress of solidification in the cavity (0.14 seconds from the entrance of the melt).

MODELING SHL FORMATION

A model for the SHL was developed based on the experimental results and discussions.[5,6] First, the oxide instantaneously dissociates at the interface. Oxygen or suboxide that evolved just after pouring the melt is readily absorbed by the titanium alloy. The process proceeds depending on the stability of the oxide (Figure 2) and stops in the early stage of

solidification when a stable molding material is used. Second, oxygen evolved at the interface diffuses into cast parts being controlled by the temperature at the melt/mold material interface, where temperature and the diffusion coefficient are lowest. Metallic constituents dissociating from the oxide, however, may form a thinner enriched layer due to diffusivity less than that of oxygen. Accordingly, measures to reduce the SHL may include control of the unstable oxides at as low a level as possible; the use of a more stable oxide, such as prereduced Y_2O_3 or ZrO_2; and the suppression of the interface temperature by lowering the mold preheating temperature and applying a chilling block.

MOLD FILLING

Mold-Filling Behavior

Melt-flow and mold-filling behavior under the horizontal centrifugal force field (0–30 G) were examined by casting experiments in which the amount of the alloy melted and poured at 1,950 K (±50) and 0.8 Pa in an electron-beam furnace was adjusted to less than that required for the complete filling of the casting tree.[7,9] In a typical outlook of the cast parts, shapes of two simple-cast parts in a tree consisting of two mold cavities ($80 \times 80 \times 10\ mm^T$ with a gate of $40^W \times 20^L \times 10\ mm^T$) were nearly the same.

The cross-sectional view of the solidified shell at the inside walls of the gate and mold cavity shown in Figure 3 suggests the flow pattern of the melt to be as follows. First, melt flows into mold cavities with a velocity that increases with distance from the axis of rotation in the counterclockwise direction, keeping contact with the vertical walls of the gates and cavities on the antirotation side. Second, solidification at the vertical walls is retarded (Figure 3), and only several ten percentages of the cross-sectional area of the gate is used for the melt flow. Third, cavity filling proceeds prior to that of the gates and runner under the centrifugal force field. As this results, solidification proceeds mainly from the far end of the cavity to the gate for the mass supplied into the cavity (i.e., in the mode of directional solidification). Finally, the thickness of the solidified shell in the upper side of the cavity is nearly the same as the lower side, suggesting that the gravitational force can be neglected under the centrifugal force field.

Casting Defects and the Effect of Centrifugal Force

A detailed examination of cast parts using a two-dimensional transmission system with fine focused x-ray beams ($10\ \mu m^\phi$) reveals three types of casting defects: those with a smooth inside surface, those with an irregular inside surface, and those with an inside surface smooth on the surface side and irregular in the half-thickness side of the part (Figure 4). Defects with a smooth inside surface in the surface side were observed in a specimen cast in a lower range of rotation (0–200 rpm) and often occupy about 10 vol.% of cast parts during static casting. These defects were considered to be gas bubbles trapped during the early stage of solidification.

The origin of gaseous defects seems to be water originally adsorbed at the inside surface of the casting mold that may evaporate just after contact with the melt and may be easily entrapped into the melt. Defects with an irregular inside surface in the core zone seem to be shrinkage cavities, in which columnar and equiaxed dendrites are often found in the half-thickness side of part, as shown in the lower right of Figure 4. This fact suggests that the residual melt in the periphery of a gas bubble may flow in the direction of solidification shrinkage, being enhanced by the centrifugal force.[7]

With an increase in centrifugal force, various kinds of defects are markedly reduced, as shown in Figure 5, in which an index of defects corresponds to the sum of the product of defect dimensions measured in the X and Y coordinates. As a result, the average density of the cast part increases with centrifugal force and becomes very close to the theoretical density in the range of 20–40 G. The tensile strength of specimens simultaneously cast, machined, hot isostatically pressed (7.2 ks at 1,223 K, 101 MPa), and heat treated at 1,223 K for 36 ks increased from 838 MPa at 2 G to 878 MPa at 20 G, which is in the range specified by ASTM.

Mold Filling and Solidification Simulation

The process sequence during the centrifugal casting of 6 kg of molten titanium alloy occurs in a short time—pouring from a skull crucible, 1.0; falling into the runner, 0.4; mold filling into the cavities, 1.0; and solidification, 12.[9]

The mold-filling process has been analyzed using the Navier-Stokes equation and the equation for continuity as the basic equations in a two-dimensional plane by assuming free surface flow. The methods adopted were the solution-algorithm method for time integration, the finite-differential method for space integration, and the volume of fluid method for the tracking of the free surface. The velocity of the melt is set to be zero in the free surface of the melt on the line (S-S′ in Figure 6). It is assumed that the melt in contact with the mold cavities is accelerated by the centrifugal force, $(\text{density})x\ (X_C - X)^2$, under friction between the melt and the mold cavities with a friction coefficient of 0.2–0.4. It is also assumed that the melt, without any contact with the cavity surface, receives reduced centrifugal force. Calculations were made using

(Continued on page 34.)

References

1. M.J. Donachie, *Titanium, A Technical Guide* (Material Park, OH: ASM, 1988).
2. D. Eylon, *Proc. 2nd Japan Intern. SAMPE Symp. and Exhibition* (Chiba, Japan: 1991), p. 351.
3. D. Eylon, J.R. Newman, and J.K. Thorne, *Metals Handbook,* 10th ed. (Materials Park, OH: ASM, 1991), p. 634.
4. S. Watakabe, K. Suzuki, and K. Nishikawa, *ISIJ Intern.,* 32 (1992), p. 625.
5. K. Suzuki, K. Nishikawa, and S. Watakabe, *Trans. JIM,* 60 (1996), p. 734.
6. K. Suzuki, K. Nishikawa, and S. Watakabe, *Materials Trans. JIM,* 38 (1997), p. 54.
7. K. Suzuki, K. Nishikawa, and S. Watakabe, *Materials Trans. JIM,* 37 (1996), p. 1793.
8. K. Oi, H. Terashima, and H. Toda, *Imono,* 66 (1994), p. 3.
9. K. Oi, H. Toda, and H. Terashima, *Imono,* 65 (1993), p. 827.
10. K. Oi, H. Terashima, and K. Suzuki, *Metallurgy and Technology of Practical Titanium Alloys,* eds. S. Fujishiro, D. Eylon, and T. Kishi (Warrendale, PA: TMS, 1994), pp. 219–224.
11. I. Barin et al., *Thermodynamic Properties of Inorganic Substances* (New York: Springer-Verlag, 1973).
12. J.L. Murray, *Phase Diagrams of Binary Titanium Alloys* (Materials Park, OH: ASM, 1987).
13. K. Suzuki and K. Sanbongi, *Trans. ISIJ,* 15 (1975), p. 618.
14. H. Niiyama et al., *J. of the Less-Common Metals,* 169 (1991), p. 209.
15. N. Sakuma et al. *Tetsu-to-Hagane,* 78 (1992), p. 680.
16. M. Hoch, *Titanium, Science and Technol.,* (Oberursel, Germany: DGM, 1984), p. 1431.
17. R.L. Saha et al., *Met. Trans. B,* 21B (1990), p. 559.
18. S.R. Lyon and S. Inoue, *Titanium, Science and Tech.,* eds. R.I. Jaffee and H.M. Burte (1973), p. 239.
19. L. Wictorin, N.El. Mahhalawy, and H. Fredrikson, *Cast. Metals,* 4 (1992), p. 182.
20. C.J. Rosa, *Met. Trans. B,* 1B (1970), p. 2517.
21. R.J. Wasilewski and G.L. Kehl, *J. Inst. Metals,* 83 (1954), p. 94.
22. R. Mehrabian, M. Keane, and M.C. Flemings, *Met. Trans. B,* 1B (1970), p. 1209.
23. T. Takahashi and I. Ogiwara, *Trans. JIM,* 29 (1965), p. 1152.